White Rose Research Online

eprints@whiterose.ac.uk
https://eprints.whiterose.ac.uk
Universities of Leeds, Sheffield and York

Deposited via The University of Sheffield.

White Rose Research Online URL for this paper:
https://eprints.whiterose.ac.uk/id/eprint/235009/

Version: Published Version

Article:
Wickham, B., De-Ville, S. and Stovin, V. (2025) The estimation of evapotranspiration rates from urban green infrastructure using the three-temperatures method. Hydrology, 12 (12). 315. ISSN: 2306-5338

https://doi.org/10.3390/hydrology12120315

Reuse
This article is distributed under the terms of the Creative Commons Attribution (CC BY) licence. This licence allows you to distribute, remix, tweak, and build upon the work, even commercially, as long as you credit the authors for the original work. More information and the full terms of the licence here: https://creativecommons.org/licenses/

Takedown
If you consider content in White Rose Research Online to be in breach of UK law, please notify us by emailing eprints@whiterose.ac.uk including the URL of the record and the reason for the withdrawal request.

UNIVERSITY OF LEEDS
University of Sheffield
UNIVERSITY of York

hydrology

MDPI

Article

The Estimation of Evapotranspiration Rates from Urban Green Infrastructure Using the Three-Temperatures Method

Bruce Wickham [1], Simon De-Ville [2] and Virginia Stovin [1,*]

[1] School of Mechanical, Aerospace, and Civil Engineering, The University of Sheffield, Sheffield S1 4DT, UK
[2] Department of Civil & Environmental Engineering, University of Liverpool, Liverpool L69 3GH, UK
* Correspondence: v.stovin@sheffield.ac.uk

Abstract

The three-temperatures (3T) method is a robust approach to estimating evapotranspiration (ET), requiring relatively few measurable, physical parameters and an imitation surface, making it potentially suited for estimating ET from sustainable drainage systems (SuDS) and green infrastructure (GI) in urban environments. However, limited 3T-ET data from SuDS and/or GI makes it difficult to assess the conditions that affect its accuracy. The purpose of this study was to determine whether reasonable ET estimates could be achieved using the 3T method with a plastic imitation surface for a small, homogenous vegetated surface. The 3T-ET estimates were produced at an hourly timestep and compared to reference ET (ET_o) derived using the Penman–Monteith equation. The 3T-ET estimates were consistently higher than ET_o (mean absolute error of 0.05 to 0.15 mm·h^{-1}), which may indicate systematic overestimation of ET or that the actual ET was greater than ET_o. Unrealistic 3T-ET estimates are produced when the air temperature and the imitation surface temperature converge, limiting the method's application to between mid-morning and late afternoon. Further work to validate and refine the 3T method is required before it can be recommended for deployment in the field for spot-sampling ET rates from urban SuDS/GI.

Keywords: three temperatures (3T); evapotranspiration (ET); sustainable drainage systems (SuDS); green infrastructure (GI); remote sensing (RS)

check for updates

Academic Editor: Evangelos Rozos

Received: 14 October 2025
Revised: 14 November 2025
Accepted: 24 November 2025
Published: 27 November 2025

Citation: Wickham, B.; De-Ville, S.; Stovin, V. The Estimation of Evapotranspiration Rates from Urban Green Infrastructure Using the Three-Temperatures Method. *Hydrology* **2025**, *12*, 315. https://doi.org/10.3390/hydrology12120315

Copyright: © 2025 by the authors. Licensee MDPI, Basel, Switzerland. This article is an open access article distributed under the terms and conditions of the Creative Commons Attribution (CC BY) license (https://creativecommons.org/licenses/by/4.0/).

1. Introduction

Evapotranspiration (ET) plays a key role in the redistribution of water in the hydrological cycle [1]. In sustainable drainage systems (SuDS), a form of green Infrastructure (GI) designed for stormwater management, ET plays a vital role in reducing the volumes of stormwater, thereby helping to alleviate flood risks. Numerous studies have attempted to quantify ET rates from typical SuDS configurations [2–6]. These studies typically demonstrate that measured ET rates differ significantly from the reference ET (ET_o) rates calculated using the Penman–Monteith (PM) FAO56 formula. Accurate estimation of ET from SuDS is complicated by three interacting factors: (i) The types of vegetation used differ from traditional crops, and they are often characterised by structurally varied planting mixes such that well-established crop factors (K_c) may not be transferable; (ii) moisture content in SuDS will not always be maintained under 'well-watered' conditions such that a water stress coefficient (K_s) may be required; and (iii) SuDS plan areas may be small compared with a homogeneous field setting such that a third factor (K_l) may be required to represent local microclimate—or urban setting—factors. To further our understanding of how these three factors combine to determine actual ET rates from urban SuDS in practice requires

a measurement technique that can be applied in situ, i.e., the ultimate aim is a portable system that might be taken out into the field to spot sample ET rates associated with SuDS/GI installations. The main aim of the present paper is to determine whether the 'Three-Temperatures' (3T) method could provide that capability.

1.1. Traditional Methods for Quantifying ET

Several methods of quantifying ET from a surface exist, each having advantages and disadvantages and some being better suited than others for particular applications and situations, as summarised in Shuttleworth [7] and Abtew and Melesse [8]. Direct methods of measuring ET include (but are not limited to) lysimetry, evaporation pans, water balance, soil moisture depletion, leaf porometry, and sap flow measurements [7]. However, these are typically better suited to homogenous crops, and many require costly and specialised equipment, are difficult to physically implement, are intrusive/disturb the system of interest, and/or present a challenge for up-scaling [7,8].

Indirect and remote sensing methods include eddy covariance, infrared scintillometry, and the Bowen ratio. Eddy covariance requires specialised and costly instrumentation to monitor the wind speed in the vertical and horizontal plane, as well as gas concentrations above a vegetated surface [9]. This method works best when the wind speed, air temperature, humidity, and CO_2 are steady and the vegetation surface is flat and homogeneous [9]. Infrared scintillometry also requires specialised equipment, including a pair of large-aperture scintillometer instruments (emitter and receiver), and it is better suited to applications covering large, flat areas (e.g., distances over several hundred metres) exhibiting a moderate range of atmospheric turbulence and minimal variation in spatial climatic conditions [10]. The Bowen ratio method requires measurements of temperature and vapour pressure at two heights above the vegetated surface [11]. The temperature and humidity gradients measured by Bowen ratio instruments reflect the energy balance of the upwind surface. The measurements must be made within the 'constant flux layer', a boundary layer of the atmosphere where the turbulent fluxes are assumed to be constant with height. The fetch must be long enough for this layer to fully develop over a uniform surface. The ideal fetch-to-height ratio is often cited as 100:1 [12]. This requirement for uniform upwind surface conditions is incompatible with the size and heterogeneous nature of typical urban SuDS and GI devices.

1.2. Three-Temperatures Method

The Three-Temperatures (3T) method, originally developed by Qiu et al. [13], provides an alternative approach that may be more readily applicable to SuDS and other forms of GI. It requires a few readily measurable physical parameters that can be obtained in situ or via remote sensing, making it relatively easy to deploy in the field at different spatial scales and settings. The 3T method solves for the latent heat component ($Q_{LE,veg}$) in the simplified surface energy balance for the vegetated surface of interest and relates this to the energy available to drive ET. The 3T method requires five parameters, specifically the net radiation from the vegetated surface ($Q_{Rn,veg}$) and the imitation surface ($Q_{Rn,imt}$) alongside the surface temperatures from the vegetated surface (T_{veg}) and corresponding imitation surface (T_{imt}) together with the overlying air temperature (T_{air}), as shown in Figure 1.

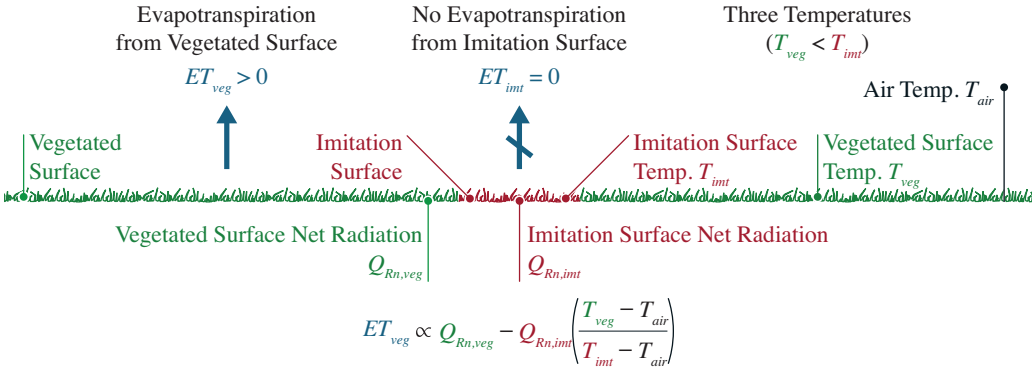

Figure 1. A conceptual diagram of the three-temperatures method.

The 3T method has met with varying degrees of success. Zhang et al. [14] applied the 3T method to estimate ET from small, isolated green roofs and permeable paving systems (<0.36 m^2) located on weighing platforms (for validation purposes) in an urban environment. Their study reported a coefficient of determination (R^2) between 0.6 and 0.7 and mean absolute errors (MAEs) between 0.06 and 0.12 $mm \cdot h^{-1}$. However, low accuracy of the 3T method was observed during the early morning and late afternoon due to low air temperature and low solar radiation [14]. Qiu et al. [15] compared 3T-ET estimates with those derived from the Bowen ratio method above a grass field (approximately 300 m in diameter) in the city of Shenzhen. Comparisons of hourly ET estimates showed R^2 values between 0.89 and 0.95 and root mean square error (RMSE) values between 0.03 and 0.04 $mm \cdot h^{-1}$. Qiu et al. [16] compared the estimates of 3T transpiration values, based on a three-dimensional adaption of the original 3T method, to transpiration estimates produced by stable isotope partitioning for an urban shrub located on the roof of a building in Shenzhen. The results of the comparison showed an R^2 value of 0.61 and an MAE of 0.1 $mm \cdot h^{-1}$ [16].

1.3. Knowledge Gaps for 3T-ET

In the context of determining whether the 3T method might be suitable for spot-sampling ET rates from urban SuDS/GI in situ, two key knowledge gaps have been identified. These are as follows: (i) when, during a daily cycle, the estimation technique can reliably be applied; and (ii) whether a plastic reference surface might provide a more robust option compared with previous paper-based approaches. These two knowledge gaps are expanded upon below, leading to the development of a unique experimental facility that allows the data required to undertake 3T estimates to be recorded continuously over a period of several months.

Many of the 3T-ET studies only report 3T-ET estimates over short periods of time and typically only during the middle of the day. Qiu et al. [15] reported hourly values over three days, Tian et al. [17] compared only 7 hourly 3T-ET estimates, and Qiu et al. [16] compared only 13 estimates of hourly 3T-ET between 10:03 and 12:28. Limited 3T-ET data provide reduced insight into the performance of the method and fail to fully explain the conditions or factors that affect its accuracy, including local meteorological conditions and changes in the environmental setting. This could be addressed through the continuous recording of 3T-ET input parameters over longer time periods, allowing an understanding of the circumstances under which credible and less-credible estimates of 3T-ET are produced.

A key consideration for producing continuous records for 3T-ET estimates is the imitation surface. For some of the 3T studies [14,16,18], the imitation surface used was a green printed paper resembling vegetation. However, this surface had to be covered/replaced due to rainfall/unfavourable conditions, making it impractical for continuous monitor-

ing. Alternatively, the surface temperature for the imitation surface was taken from the maximum value (i.e., 'hot-spot' or 'hot pixel') observed on the surface itself [15,19], which assumed that no ET was occurring from that surface at that time. Zou et al. [19] recognised that this assumption may result in the overestimation of 3T-ET and highlighted the need for an idealized imitation surface combined with automatic infrared remote sensing to be used in continuous measurements at a high frequency.

Aside from work directly related to the 3T method, infrared thermography is regularly used within the agricultural and plant science community to determine plant stress and/or support irrigation scheduling. As with the 3T method, comparisons are made between the healthily transpiring crop and a dry reference surface, assuming that this dry reference has similar aerodynamic (e.g., size, roughness and orientation) and optical (absorptance and exposure to incoming radiation) properties to the leaf of interest. Dry reference surfaces have included real leaves covered in petroleum jelly (Vaseline), which blocks all transpiration [20], cellulose paper-based hemispherical surfaces [21], and thin plastic hemispherical surfaces [22,23]. Jones et al. [22] noted that flat reference surfaces do not represent the range of illumination experiences by typical leaves well. They used a thin plastic hemispherical reference surface with the temperature sensor mounted inside. Analyses were also undertaken to ensure that the shade of green paint used matched the solar absorptivity/albedo of the vegetation. It is therefore proposed that a green plastic artificial grass surface may meet the requirements for an artificial dry reference surface in the current context.

1.4. Aims and Objectives

Evidence from the literature demonstrates there is a need to improve our understanding of the 3T method's limitations and confirm its ability to produce robust estimates of ET at sub-daily timesteps. Therefore, this study aimed to determine whether reasonable ET estimates can be achieved using the 3T method and a plastic imitation surface for a small, homogenous, vegetated surface analogous to SuDS and/or GI. The objectives of the study were as follows:

1. Reproduce the 3T method for a homogenous vegetated surface (grass), producing a continuous record of ET estimates using a plastic artificial grass imitation surface;
2. Determine the sensitivity of the 3T method to key parameters, specifically identifying potential limitations and practical considerations;
3. Comment on the fit of 3T-ET hourly estimates to corresponding reference ET values derived from Penman–Monteith (PM) (FAO-56).

2. Materials and Methods

The 3T experiment was set up for a homogenous surface of a standard amenity grass turf mat, established on a porous substrate media, analogous to a green roof system. The experiment was located on a third-floor roof terrace of the University of Sheffield's Sir Robert Hadfield Building, Sheffield, United Kingdom (53.381693° N; 1.477279° W; elevation 95 mAOD). The primary data was collected at a one-minute timestep between October and November 2023 and from January to March 2024.

2.1. Experimental Setup

The experimental setup included two test beds: a net radiation test bed and an imitation surface test bed (Figure 2a). The test beds comprised a gently sloping (approximately 2° slope) hard plastic sealed tray with an outlet drainpipe, lined with a permeable geotextile (PermaSEAL Green Roof Root Barrier Membrane) above a drainage layer (PermaSEAL PRO 8 Green Roof Drainage Membrane) on the bottom surface.

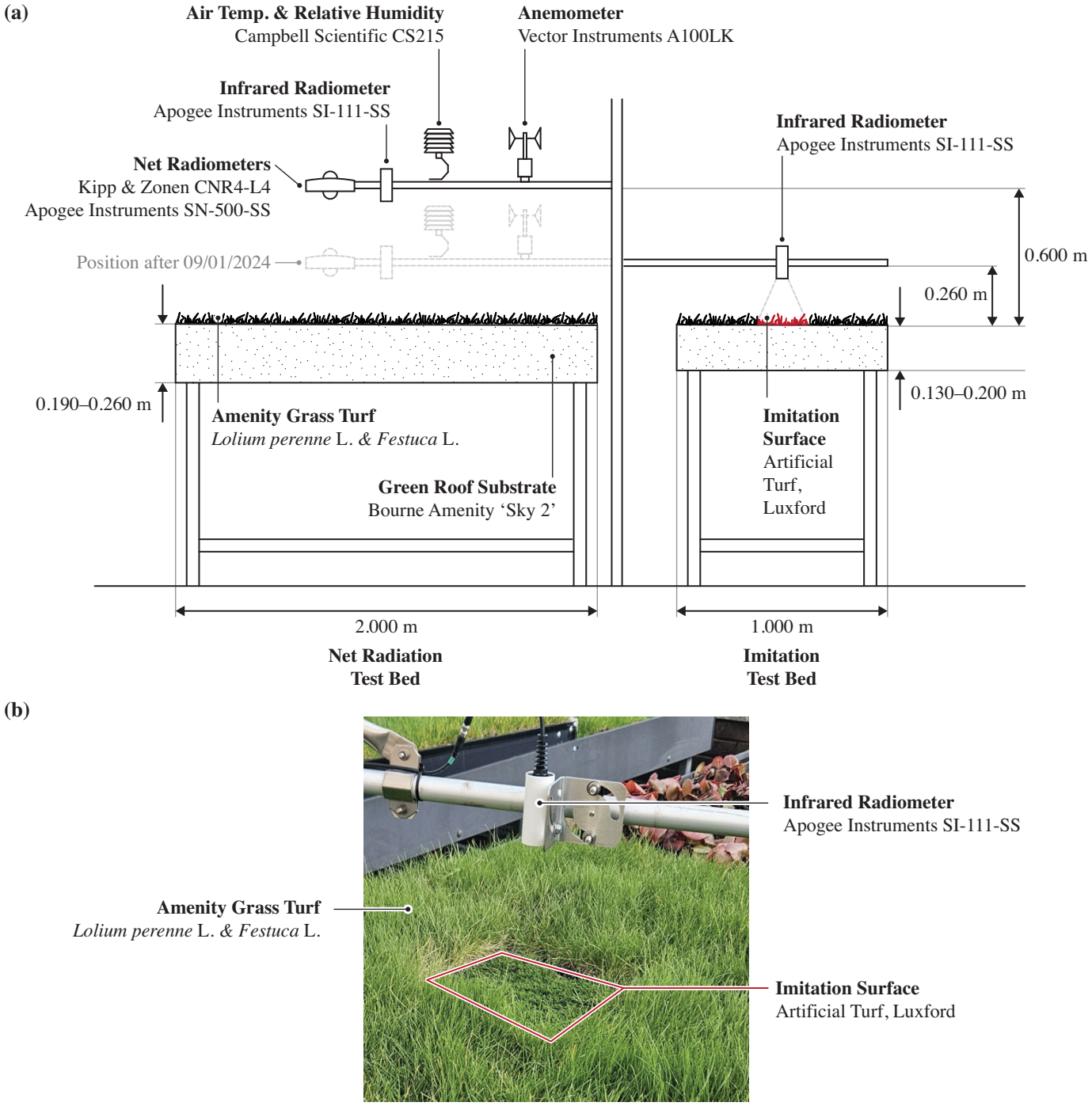

Figure 2. (**a**) Transverse cross-section of the study test beds. (**b**) The imitation surface embedded in the grass turf surface of the imitation test bed.

These test beds were filled with a commercially available green roof substrate (Bourne Amenity 'Sky 2' Green Roof Substrate). The surface of the substrate mix was made level by introducing plastic retaining boards along the lower edges of the test bed. Hence, substrate depths varied between 190–260 mm and 130–200 mm for the net radiation and imitation surface test beds, respectively. This substrate mix was chosen to ensure that the experimental setup was representative of vegetated SuDS in practice and minimise the possibility of water ponding on the surface of the vegetation (ponded water would result in unrealistic/unfavourable conditions for the 3T method).

The substrate in both test beds was covered by a standard amenity grass turf mat (approximately 25.0 mm thick), comprising a mixture of *Lolium perenne* L. 'ryegrass' and *Festuca* L. 'fescue-grass'. This vegetation cover was chosen for the following reasons:

- It mimics the standard homogenous grass surface characteristics required to calculate the reference ET from a grass surface following the PM FAO-56 method;
- The vegetation is robust throughout all seasons and resilient to changing weather conditions;
- The vegetation is easy to maintain to ensure near 'constant' surface characteristics in order to minimise experimental error;
- The vegetation has a consistent high surface coverage to minimise direct energy loss to the substrate (i.e., soil heat flux density) and minimise experimental error.

Throughout October and November 2023, grass vegetation was irrigated weekly. No irrigation was undertaken from January to March 2024 given the high rainfall conditions associated with these winter months.

The net radiation test bed covered an area of 4 m^2 (2 m $\times$ 2 m). It was monitored with a net radiometer (CNR4-L4, Kipp & Zonen, Delft, The Netherlands), infrared radiometer (Sl-111-SS, Apogee Instruments, Logan, UT, USA), shielded air temperature and relative humidity sensor (CS215, Campbell Scientific, Logan, UT, USA), and three-cup wind anemometer (A100LK, Vector Instruments, Rhyl, UK) (Figure 2a). All instruments were initially installed 0.600 m above the test bed surface. A second net radiometer (SN-500-SS, Apogee Instruments) was installed alongside the CNR4-L4 on 9 January 2024. At this time, all instruments were lowered to 0.260 m above the test bed surface. The SN-500-SS has a 180° field of view (FoV) for the incoming radiation and 150° FoV for the outgoing radiation for both shortwave and longwave radiation. This allowed for more focused measurements of net radiation from the vegetated surface compared to the CNR4-L4, which has a 180° FoV for both the incoming and outgoing radiation sensors. The accuracy and precision of the aforementioned instrumentation are provided in Supplementary Material Section A.

The imitation surface test bed had a surface area of 1 m^2 (1 m $\times$ 1 m). The imitation surface (i.e., artificial grass: Luxford, Figure 2b) was set on a modular cell located in the centre of the test bed and represented a relatively small area (0.250 m $\times$ 0.250 m, 0.0625 m^2), which contributed only 6.25% of the total test bed area. This satisfied a key assumption of the 3T method, whereby the imitation surface should not significantly alter the microclimatic conditions of the vegetated surface. Figure 2b shows that the plastic dry reference surface represents the amenity grass well in terms of the colour, texture, roughness, and orientation of the leaf structure. The surface temperature of the imitation surface was monitored with an infrared radiometer (Sl-111-SS, Apogee Instruments) mounted 0.260 m above the test bed surface (Figure 2a). The modular cell of the imitation surface was isolated/sealed (horizontally) from the adjacent test bed material to prevent the horizontal ingress of water into the cell and minimise experimental error.

2.2. Data Collection

The following physical parameters were collected at one-minute timesteps: the net radiation of the vegetated surface ($Q_{Rn,veg}$), the surface temperature of the vegetated (T_{veg}) and imitation (T_{imt}) surfaces, air temperature (T_{air}), relative humidity (RH), and wind speed (u). It should be noted that net radiation from the imitation surface ($Q_{Rn,imt}$) was not measured directly. This is due to the small surface area associated with the imitation surface. Neither of the net radiometers has a sufficiently narrow field of view to focus solely on this small patch of imitation vegetation. Mounting the sensor closer to the surface was considered, but this has serious implications on shading, and it was therefore not considered to be a sensible option.

The collected data were used to describe the local microclimate and calculate the 3T-ET estimates and hourly reference ET_o from the vegetated surface via the PM method outlined in FAO-56 [24]. The ET_o values provide a benchmark to compare the 3T-ET estimates and provide some level of assurance/confidence in the derived 3T-ET values. The grass was maintained at a height of approximately 0.120 m, watered weekly, and fertilised to ensure that the vegetation was not stressed during the data collection period, as outlined in Allen et al. [24].

Daily rainfall depths were obtained from the Environment Agency's online 15 min timestep rainfall records database [25]. These were taken from the nearest rainfall station (ID: 082732) adjacent to Ringinglow Road, Sheffield, approximately 5.60 km southwest of the study site. This rainfall data was used to distinguish between dry and wet conditions in the measured data records, in addition to in-person observations made at the study site.

2.3. Baseline 3T-ET

A baseline 3T-ET approach, referred to as ET1, was used to produce continuous estimates of 3T-ET at hourly timesteps. The hourly 3T-ET values were derived from the mean of 60 one-minute values of each relevant parameter across the corresponding hour.

In the absence of direct measurements of net radiation from the imitation surface ($Q_{Rn,imt}$), these values were estimated using established techniques. For the purpose of using consistently derived net radiation (Q_{Rn}) values, the same method was used to derive values of net radiation from the vegetated surface ($Q_{Rn,veg}$), despite monitored values being available. In this study, the sign convention for the radiation flux densities at the surface was considered 'positive' for incoming (↓) energy and 'negative' for outgoing energy (↑), which includes reflected and emitted energy.

Net shortwave radiation ($Q_{Rn,sw}$, $W{\cdot}m^{-2}$) was quantified using a fixed value of albedo (α, unitless) and incoming measured solar radiation ($\downarrow R_{solar}$, $W{\cdot}m^{-2}$):

$$Q_{Rn,sw} = (1 - \alpha) \downarrow R_{solar} \quad (1)$$

An α value of 0.230 was used based on the recommended default value for the green reference grass provided in Allen et al. [24]. $\downarrow R_{solar}$ was taken as the measured incoming shortwave radiation recorded at the test beds; between October and November 2023, this was taken from values measured by the CNR4-L4 instrument and from SN-500-SS for January to March 2024.

Net longwave radiation ($Q_{Rn,lw}$, $W{\cdot}m^{-2}$) was derived from the difference between incoming ($\downarrow R_{lw}$, $W{\cdot}m^{-2}$) and outgoing ($\uparrow R_{lw}$, $W{\cdot}m^{-2}$) longwave radiation components for the respective surfaces:

$$Q_{Rn,lw} = \downarrow R_{lw} - \uparrow R_{lw} \quad (2)$$

The $\downarrow R_{lw}$ component was taken as the measured values from the net radiometer at the test beds. The $\uparrow R_{lw}$ component included the emitted longwave radiation from the surface plus the reflected longwave radiation and was calculated via:

$$\uparrow R_{lw} = \epsilon\sigma(T)^4 + (1 - \epsilon) \downarrow R_{lw} \quad (3)$$

The emitted longwave radiation was estimated using a fixed emissivity value (ϵ, unitless) taken as 0.900 based on the default value for short grass [26] (the impact of using the same value of α (0.230) and ϵ (0.900) for both surfaces is explored later in this article), the Stefan–Boltzmann constant (σ, 5.6697×10^{-8} $W{\cdot}m^{-2}{\cdot}K^{-4}$), and the corresponding surface temperature (T, K), as outlined in the Stefan–Boltzmann law. The reflected longwave radiation was estimated using the same emissivity value (0.900) and the measured $\downarrow R_{lw}$.

The resultant net radiation (Q_{Rn}, W·m^{-2}) was calculated as the sum of net shortwave and net longwave radiation:

$$Q_{Rn} = Q_{Rn,sw} + Q_{Rn,lw} \quad (4)$$

Equations (1)–(4) were used to calculate $Q_{Rn,imt}$ and $Q_{Rn,veg}$. The use of T_{imt} or T_{veg} in place of T in Equation (3) resulted in Equation (4) producing $Q_{Rn,imt}$ or $Q_{Rn,veg}$ values, respectively.

The latent heat flux density for the vegetated surface ($Q_{LE,veg}$, W·m^{-2}) was estimated by the 3T method:

$$Q_{LE,veg} = Q_{Rn,veg} - Q_{Rn,imt}\left(\frac{T_{veg} - T_{air}}{T_{imt} - T_{air}}\right) \quad (5)$$

To express the 3T-ET rate as a depth of water per unit time (mm·h^{-1}), the latent heat flux density ($Q_{LE,veg}$) was divided by the density of water (ρ_w, 997 kg·m^{-3}) and the latent heat of vaporisation (λ, J·kg^{-1}):

$$\lambda = \left(2.501 - \left(2.361 \times 10^{-3}\right) T_{air}\right) \times 10^6 \quad (6)$$

The conversion from W·m^{-2} to mm·h^{-1} was achieved via the following:

$$ET_{3T,dt}\ (\text{mm·h}^{-1}) = \left(\frac{Q_{LE,veg}\ (\text{W·m}^{-2})}{\lambda\ (\text{J·kg}^{-1})\ \rho_w\ (\text{kg·m}^{-3})}\right) \times 3.60 \times 10^6 \quad (7)$$

Noting that 1 W·m^{-2} = 1 J·s^{-1}·m^{-2} and the constant 3.60×10^6 combines the unit conversions of seconds to hours (3600 s·h^{-1}) and metres to millimetres (1000 mm·m^{-1}), the unit cancellation can be shown explicitly:

$$= \left(\frac{\text{J·s}^{-1}\text{·m}^{-2}}{(\text{J·kg}^{-1})(\text{kg·m}^{-3})}\right) \times 3600 \times 1000$$

$$= (\text{m·s}^{-1}) \times 3.60 \times 10^6 = \text{mm·h}^{-1}.$$

The 3T-ET estimates at the hourly timestep allowed for comparisons with the corresponding ET_o values, as derived by the FAO-56 PM hourly method. The ET_o rates were calculated from the measured net radiation ($Q_{Rn,veg}$) values and the corresponding mean hourly meteorological parameter values (T_{air}, RH, and u).

2.4. Sensitivity of 3T-ET

A sensitivity analysis was undertaken using the baseline 3T-ET1 method. The datum condition corresponded to 'preferred' circumstances, specifically dry conditions (no/little rainfall leading up to and during this point, minimum 1-day lead in time), relatively low wind speeds (<3.00 m·s^{-1}), a distinct surface and air temperature profile throughout the daylight hours (i.e., $T_{imt} > T_{veg} > T_{air}$), and a clear sky (relatively high incoming shortwave radiation, especially near the middle of the day). The sensitivity analysis involved changing each of the individual parameters of the 3T method whilst holding the remaining parameters unchanged (i.e., assuming independence).

In addition to the percentage change sensitivity analyses, the experimental setup was also assessed to understand how sensitive/responsive it was to changes in the environmental setting, including building shadow effects, cloud cover, and reflections from adjacent windows, all of which are relevant in an urban setting. Kendall correlation (τ) values were used to explore the relationships between surface temperatures and either incoming solar radiation or air temperature.

2.5. Variations of the 3T-ET Method

Both the vegetated and imitation surfaces have similar surface characteristics (colour, shape, and appearance). The baseline approach (ET1) used calculated values for $Q_{Rn,imt}$ and $Q_{Rn,veg}$ based on independent surface temperatures, and thus considered different values of net radiation for the two surfaces (Equations (1)–(4)). A second 3T-ET approach (ET2) was considered, in which T_{veg} was used to calculate both $Q_{Rn,imt}$ and $Q_{Rn,veg}$, assuming the net radiation to be the same between the two surfaces. A comparison between calculated values of $Q_{Rn,veg}$ with measured values is presented in Supplementary Material B, where a strong correlation between the two is clearly demonstrated.

The ET1 and ET2 3T-ET estimates are based on default values of α (0.230) and ϵ (0.900). However, in reality, these values are not necessarily constant [27,28]. As such, a third approach for calculating 3T-ET was considered (ET3), where the net radiation for the vegetated and imitation surfaces was assumed to be the same, but it was based on the measured values of $Q_{Rn,veg}$. Using the measured values of net radiation, changes in α and ϵ throughout the day would be represented in the data and 3T-ET estimates.

In the case of densely vegetated surfaces, such as in this study, the 3T method also assumes that the soil heat flux density is negligible [13]. This may be reasonable for calculating ET at a daily timestep, but there is uncertainty for sub-daily values (i.e., hourly). Hence, a fourth approach for calculating 3T-ET was considered (ET4), where net radiation values for the vegetated and imitation surfaces were the same (as per ET3), and the soil heat flux density estimates (Q_{Soil}, W·m^{-2}) were treated as energy loss from the vegetated surface. Q_{Soil} was calculated as a fraction of the corresponding $Q_{Rn,veg}$ values, which is a method outlined in Allen et al. [24]:

$$Q_{Soil} = \begin{cases} Q_{Rn,veg} \times 0.1, & Q_{Rn} \geq 0 \\ Q_{Rn,veg} \times 0.5, & Q_{Rn} < 0 \end{cases} \quad (8)$$

This is a robust approach to estimating the soil heat component in the absence of measured data. The $Q_{LE,veg}$ values were calculated by subtracting the corresponding Q_{Soil} from the measured $Q_{Rn,veg}$ values.

These four different 3T-ET estimation approaches (ET1 to ET4) were evaluated against the corresponding reference ET_o values. Five metrics were used to quantify the quality of the 3T predictions; these are (i) the mean absolute error (MAE), (ii) mean absolute percentage error (MAPE), (iii) percentage bias (PBIAS), and (iv and v) the slope (m) and coefficient of determination (R^2), respectively, of a simple linear regression with a y-intercept of 0.00.

3. Results and Discussion

Two 4-day periods of 'preferred' conditions were identified from within the data: 15–18 October 2023 and 3–6 March 2024. These periods exhibited very little/no antecedent rainfall, relatively low wind speeds (majority below 3.00 m·s^{-1}), a distinct and typical surface and air temperature profile ($T_{imt} > T_{veg} > T_{air}$), and clear skies (minimal cloud cover as indicated by incoming shortwave radiation values) during the day. The monitored meteorological data across the two 'preferred' periods at the one-minute timestep are presented in Figure 3. A comparison between these two preferred periods shows similar diurnal fluctuations and magnitudes of wind speeds (approximately 0.00 m·s^{-1} to 5.00 m·s^{-1}), radiation (approximately −60.0 W·m^{-2} to 600 W·m^{-2}), and temperatures (approximately −5.00 °C to 30.0 °C).

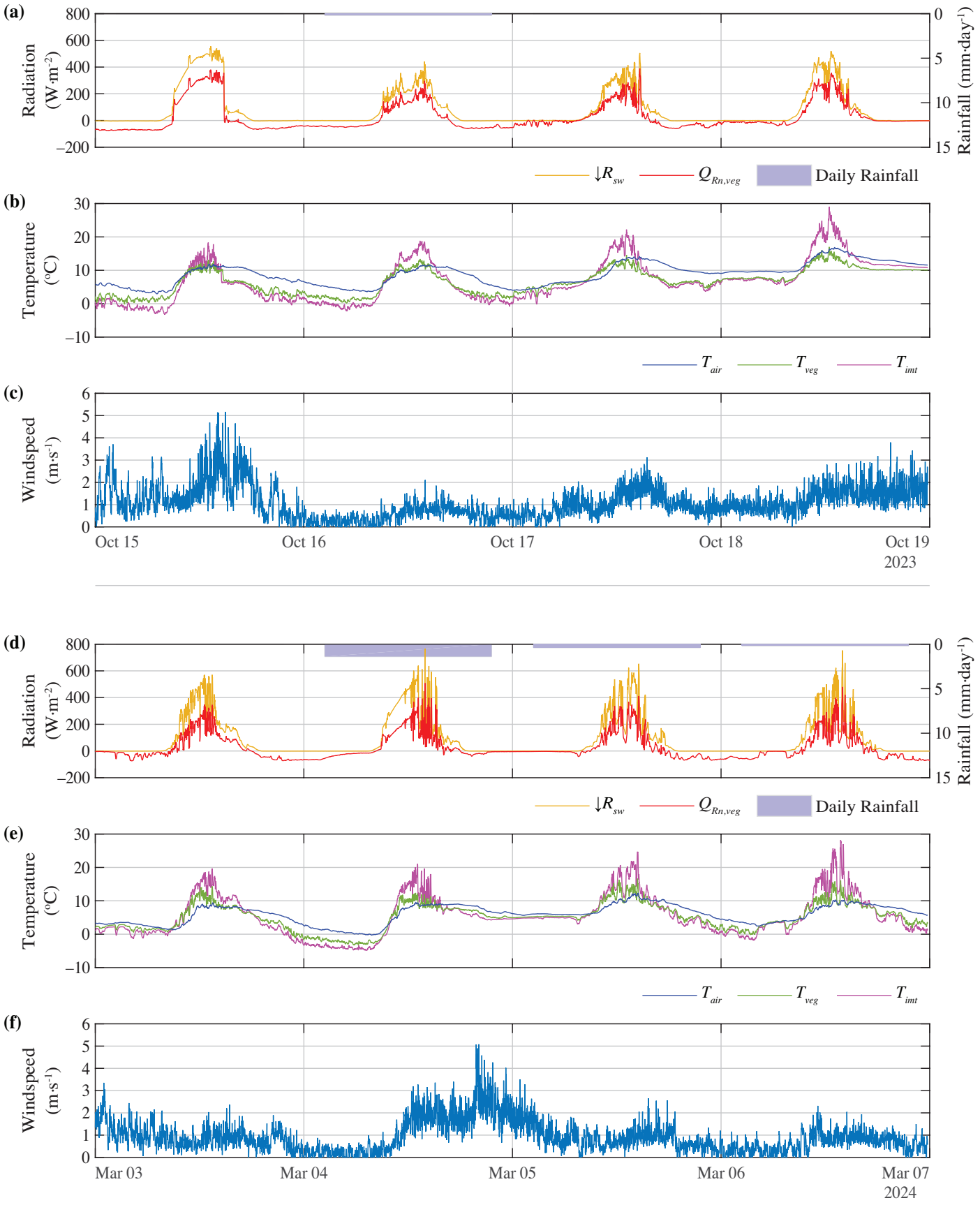

Figure 3. Two periods of preferred meteorological conditions. (**a**) October incoming radiation, (**b**) October temperature, (**c**) October wind speed, (**d**) March incoming radiation, (**e**) March air and surface temperature, and (**f**) March wind speed.

3.1. Baseline 3T-ET Estimates

The 3T-ET1 values at hourly timesteps were calculated across the preferred time periods 15–18 October 2023 and 3–6 March 2024 (Figure 4). Figure 4 also shows the hourly values of T_{veg}, T_{imt}, and T_{air} and the corresponding temperature fraction (i.e., $(T_{veg} - T_{air})/(T_{imt} - T_{air})$) for both time periods. The complete time series between 6 October and 17 November 2023 and from 13 January to 22 March 2024 is presented in Supplementary Material Section C. At 112 days, this is believed to be one of the longest continuous estimates of ET using the 3T approach in an urban environment to date, certainly without the need to cover or replace the imitation surface.

The 3T-ET1 rates were mostly positive during the day, typically reaching a maximum value soon after midday and remaining relatively constant around zero at night; this is more obvious for the October 2023 period compared to March 2024 (Figure 4c,f). There exists a clear link between the occurrence of extreme values of ET1 and the corresponding temperature fraction (where values exceed axes bounds, Figure 4c). These extreme values occurred when T_{air} and T_{imt} converged towards the same value (typically during the morning and late afternoon), as a result of temperature fluctuations over the diurnal cycle. In these situations, the temperature fraction became increasingly large (positive and negative values), resulting in extreme and unrealistic values for the corresponding ET1 rates. These phenomena are explored in more detail as part of the sensitivity analysis.

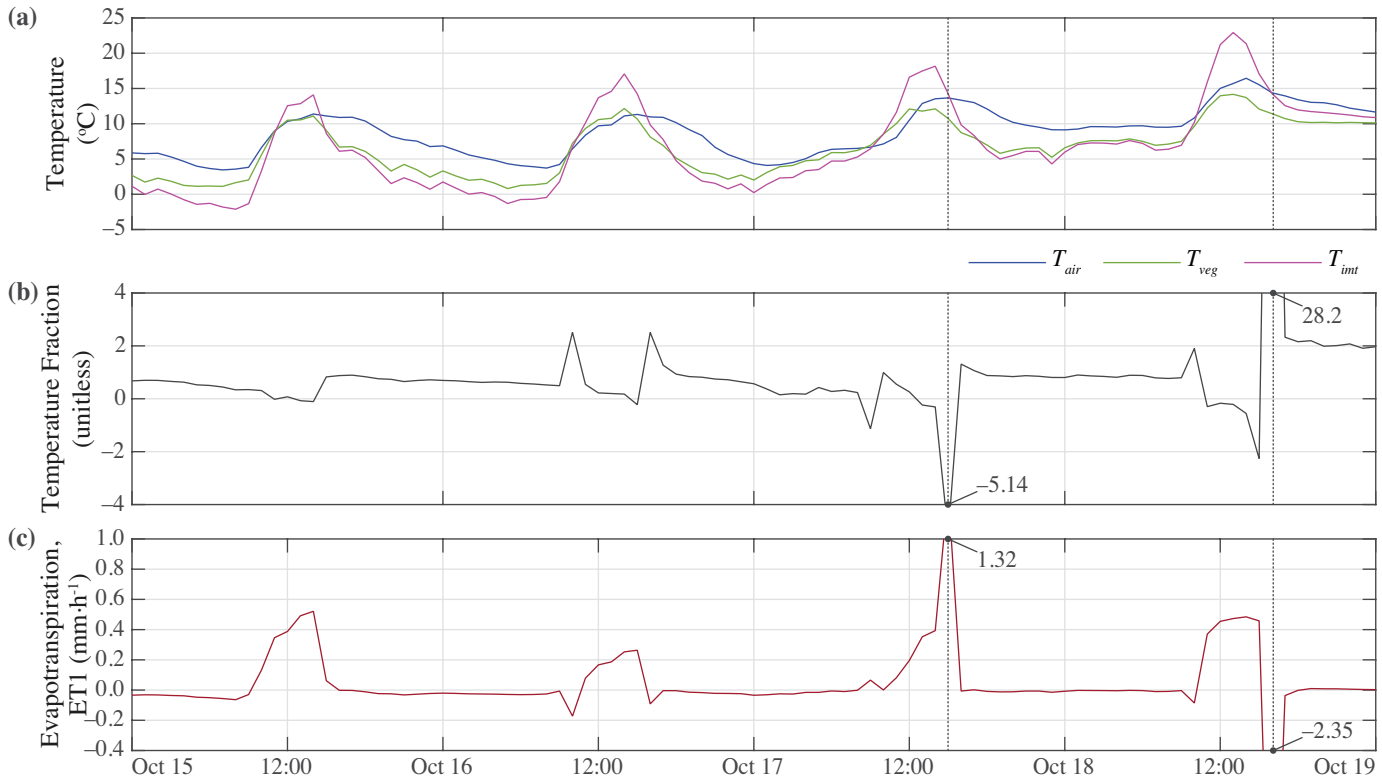

Figure 4. *Cont.*

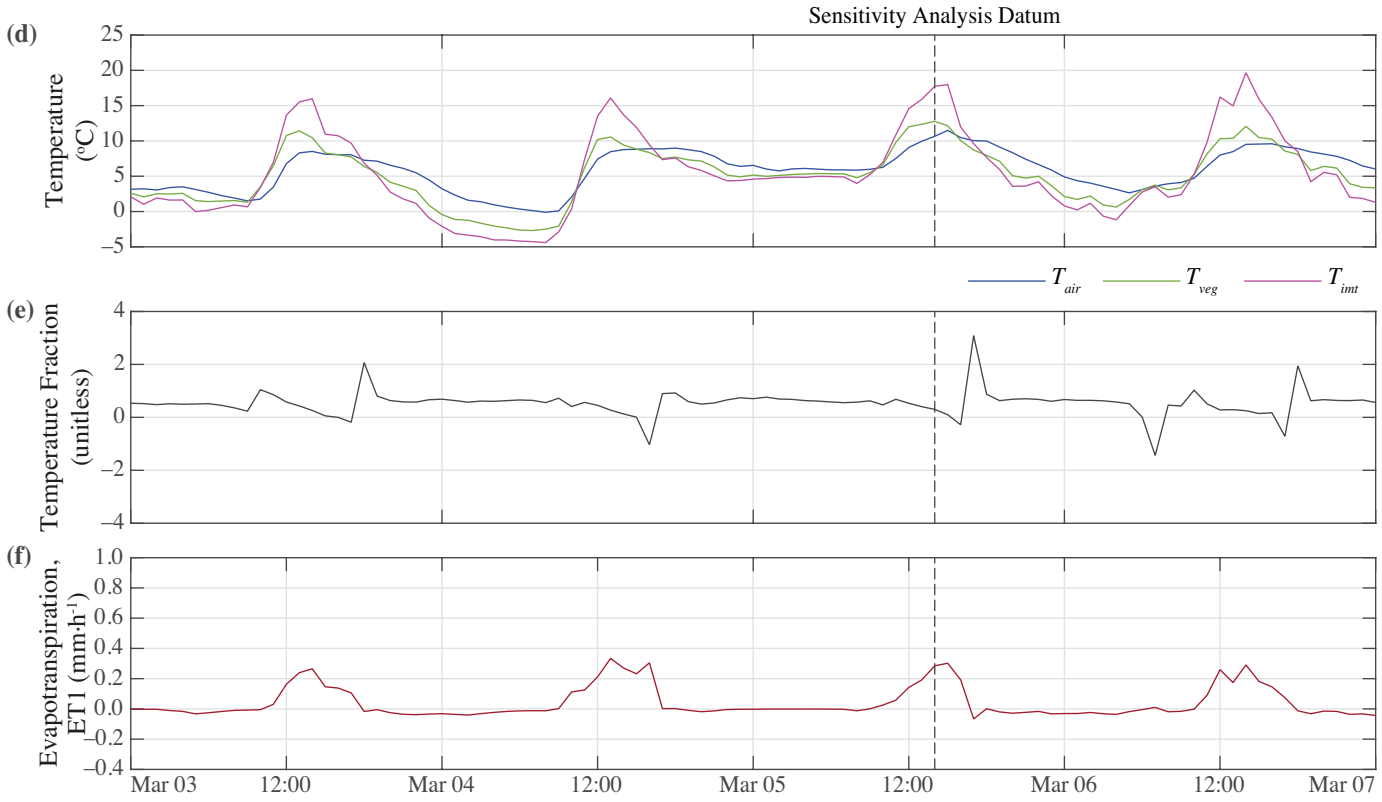

Figure 4. Comparison of hourly temperature data, 3T temperature fraction values, and 3T-ET1 estimates between 15–18 October 2023 (**a**–**c**) and 3–6 March 2024 (**d**–**f**).

3.2. Sensitivity Analysis of the 3T Method

The data recorded on 5 March 2024 at 14:00 were selected for the sensitivity analysis. This moment in time fell within the preferred period of March 2024, during which the focused net radiometer (SN-500SS) was in place (i.e., minimal interference of emitted radiation from adjacent surfaces) and not influenced by building shadows. Figure 5 shows the percentage change in the ET1 hourly estimates as a result of individually changing each 3T parameter.

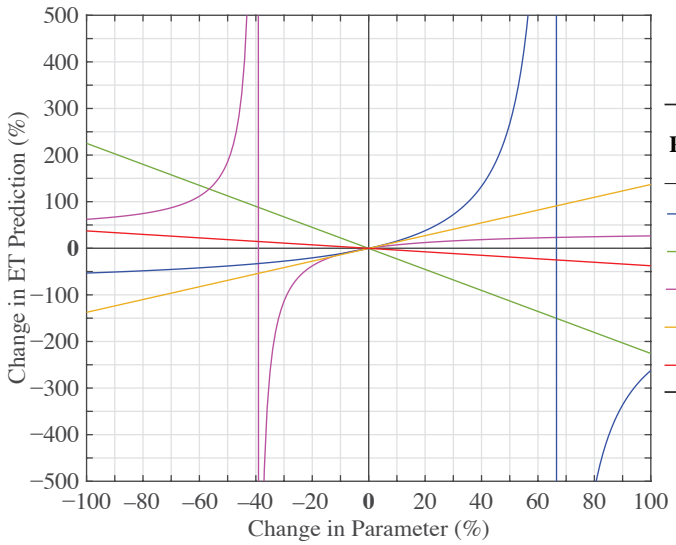

Parameter	Units	Min. Value	Datum Value	Max. Value
T_{air}	°C	0.00	10.7	21.4
T_{veg}	°C	0.00	12.8	25.6
T_{imt}	°C	0.00	17.7	35.5
$Q_{Rn,veg}$	W·m^{-2}	0.00	269	538
$Q_{Rn,imt}$	W·m^{-2}	0.00	245	490

Figure 5. Sensitivity analysis for change in 3T-ET1 (hourly) in response to independent changes in 3T parameters for 5 March 2024 at 14:00.

Figure 5 shows that ET1 estimates are particularly sensitive to changes in T_{imt} and T_{air}, specifically when the values of these parameters converge, resulting in an increasingly high temperature fraction (exponential) and extreme ET1 value. The temperature fraction is positive when T_{air} is either greater than or less than both T_{veg} and T_{imt} and negative when T_{air} is only greater than either T_{veg} or T_{imt}, but not both. This explains the typical sudden change between extreme positive and negative ET1 estimates observed when T_{air} and T_{imt} converge (Figure 4a–c 15:00 on 17/10/23 and 16:00 on 18/10/23). This high degree of sensitivity associated with the T_{imt} and T_{air} components has also been recognised in other 3T studies [14,16]. The T_{veg} parameter also impacts the ET1 estimates, exhibiting an inverse linear relationship. The remaining parameters, $Q_{Rn,veg}$ and $Q_{Rn,imt}$, have the least impact on ET1 estimates.

3.3. Robustness of the Experimental Study in the Urban Environment Setting

The experimental site was located on a rooftop at The University of Sheffield in Sheffield city centre. This urban setting created a complex microclimate environment. Figure 6 presents representative data for a single day taken on 7 October 2023, showing the diurnal shifts in the measured $\downarrow R_{sw}$, $\downarrow R_{lw}$, $Q_{Rn,veg}$, T_{veg}, T_{imt}, and T_{air}, at a one-minute timestep. This day was selected as it had mostly clear and sunny skies as determined from in-person observations and from $\downarrow R_{sw}$ radiation data.

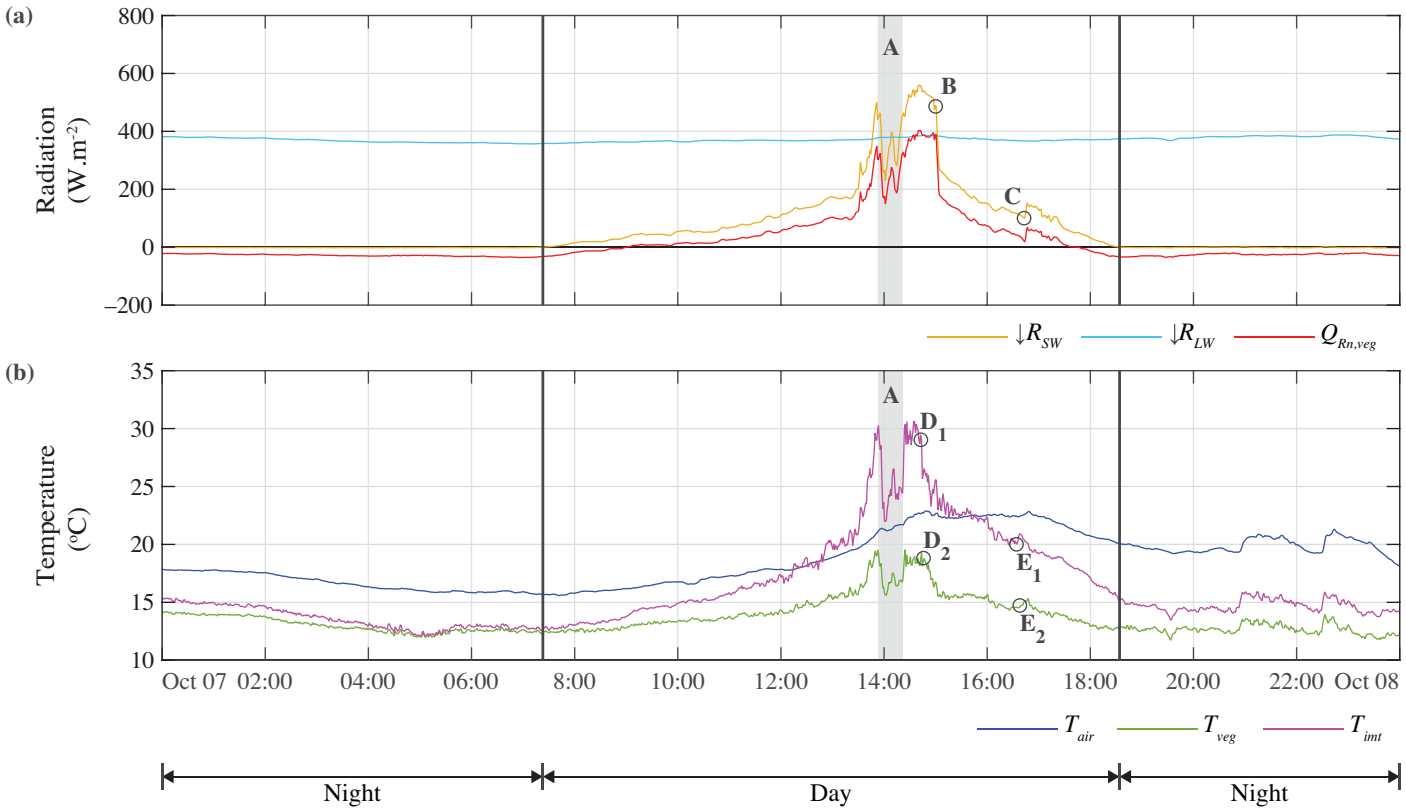

Figure 6. Diurnal fluctuations of (**a**) measured incoming shortwave and longwave radiation and net radiation and (**b**) air temperature, vegetated surface temperature, and imitation surface temperature for 7 October 2023.

A distinction between the night-time and day-time periods was made based on $\downarrow R_{sw}$ (i.e., positive values experienced during day-time), with day-time identified between 07:23 and 18:34 (British Summer Time). During night-time, variations in the surface temperatures T_{imt} and T_{veg} tended to correlate better with the prevailing T_{air} (τ between 0.42 and 0.79), whereas day-time responses correlated more closely with $\downarrow R_{sw}$ (τ between 0.80 and

0.89). There was no noticeable influence on the surface temperatures as a result of $\downarrow R_{lw}$, demonstrating that $\downarrow R_{sw}$ has the dominant impact on determining the surface temperatures during day-time. This relationship is expected in the context of the surface energy balance, providing confidence in the experimental setup's ability to capture these dynamics during continuous monitoring.

While smooth transitions might be expected in an open/rural setting, the complex urban environment of this study introduces building shadows and intermittent reflections from adjacent glass windows, in addition to the effects of cloud cover, evident from photographic records on selected days (see Supplementary Material Section D). The data shows the effects of cloud cover (time **A**, indicated by the shaded region in Figure 6) and building shadows (the period between times **B** and **C** in Figure 6a) evident from the drops in incoming radiation at 13:53–14:01 and 14:11–14:21, also observed in the changes in T_{imt} and T_{veg} (Figure 6b).

In the experimental setup, the imitation surface was located approximately 1.50 m to the west of the vegetated surface and net radiometer. This resulted in minor temporal lags observed between T_{imt} and T_{veg} in response to incoming radiation, when the sun passed behind an adjacent building. This is evident in Figure 6 where T_{imt} dropped sharply at 14:43 (time $\mathbf{D}_1$), whereas T_{veg} and $\downarrow R_{sw}$ reflected a similar decrease later at 14:46 (time $\mathbf{D}_2$) and 15:00 (time **B**), respectively. When the sun emerged from the other side of the building, it struck the imitation surface first at 16:34 (time $\mathbf{E}_1$) and then reached the net radiometer at 16:38 (time **C**).

Furthermore, the drop in surface temperature at the onset of the building shadow over the vegetated surface was also more gradual compared to the imitation surface, as shown immediately after times $\mathbf{D}_1$ and $\mathbf{D}_2$. This was for two reasons. Firstly, the area of the vegetated surface under observation was comparably larger than the imitation surface (≈640% larger) and, therefore, the building shadow had relatively more surface area under observation to progress over. Secondly, T_{veg} was noticeably lower compared to the imitation surface by ≈11 °C and, therefore, had less of a drop in surface temperature during this time period.

Figure 6 also shows a noticeable difference in the rates of change between T_{imt} and T_{veg} in response to changes in $\downarrow R_{sw}$ and T_{air} (i.e., energy inputs to the surfaces). Between 13:29 and 13:53, T_{imt} increased from 20.8 °C to 30.3 °C (45.7% change), whereas T_{veg} only increased from 15.6 °C to 19.2 °C (23.1% change). In the event of cloud cover, between 13:53 to 14:01 and 14:11 to 14:21, the resulting decrease in $\downarrow R_{sw}$ led T_{imt} and T_{veg} to decrease from 30.3 °C to 22.0 °C (27.4% change) and 19.2 °C to 15.6 °C (18.8% change), respectively. Whilst both surfaces responded to the changes in energy inputs between these times, they responded at different rates. This can be explained by the fact that the two surfaces have different material compositions and, by extension, different specific heat capacities.

For the remainder of daylight hours not affected by the building shadows (i.e., between 07:23 and 14:42), the vegetated and imitation surfaces appeared to respond very well to changes in $\downarrow R_{sw}$ and T_{air}. In the middle of the day, when the solar altitude angle was at or near its highest, there was negligible influence of spatial error introduced between the two surfaces.

In summary, the data demonstrates that the experimental setup successfully captured the diurnal cycles and changes in the 3T parameters. The data reflects the complex and dynamic environment of the surrounding urban setting at a one-minute timestep, including changes in cloud cover, transitions of building shadows and reflections from surfaces, and the shift in dominant energy inputs (i.e., $\downarrow R_{sw}$ and T_{air}) in determining the surface temperature of the relevant surfaces. The data also demonstrates the importance of instrumentation positions relative to each other and their surrounding environment, especially concerning

building shadows. At the hourly timestep used for the evaluation of the 3T method in this study, extra care is required when interpreting 3T-ET data during periods of differential shading caused by urban topology (e.g., object/building shading).

3.4. Comparison of Hourly 3T-ET Estimates and Reference ET

Four variations of the 3T-ET method (i.e., ET1, ET2, ET3, ET4) were compared across the two preferred periods of monitored data, as shown in Figure 7. As outlined in the previous sections, the site is subject to building shadows in the afternoon, and the 3T-ET method is particularly sensitive to changes in the surface and air temperatures (i.e., the temperature fraction). To avoid experimental errors and unrealistic estimates of 3T-ET values, the data for the preferred periods were filtered, as denoted by the solid plot lines shown in Figure 7, based on the following criteria: (i) exclusion of night-time periods (identified when Q_{Rn} was negative); (ii) exclusion of building shadowing in the afternoon (identified when $\downarrow R_{sw}$ drops rapidly around 15:00); and (iii) exclusion of periods when T_{imt} and T_{air} converge (identified when the absolute temperature fraction is greater than ± 1). This filtering process ensured that only 3T-ET estimates from the middle of the day, where the ET rates would be at their highest, were considered. The number of valid data points after each filter application is presented in Table 1.

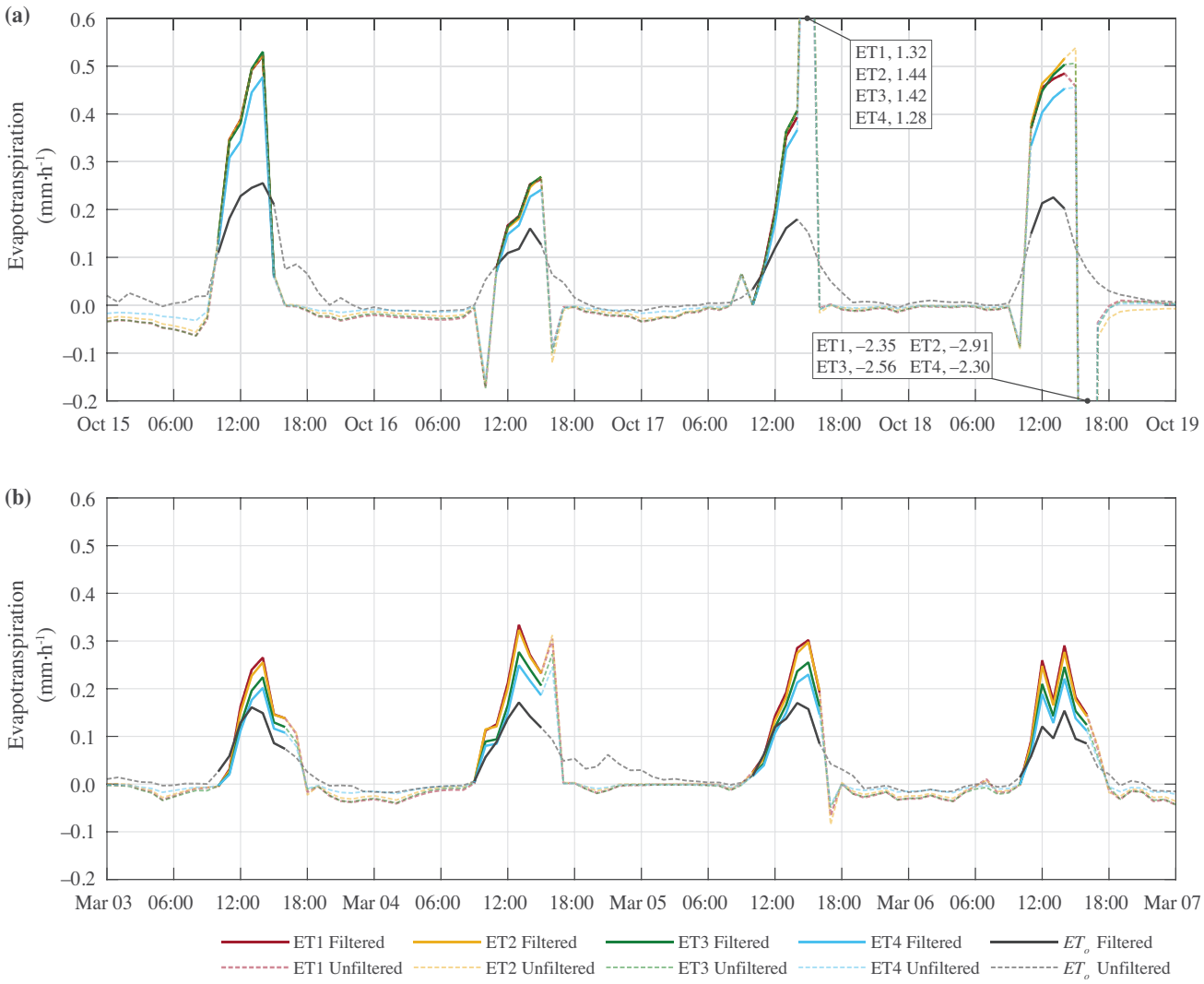

Figure 7. Hourly 3T estimates for ET1, ET2, ET3, and ET4 and reference ET between (**a**) 15–18 October 2023 and (**b**) 3–6 March 2024.

Table 1. Number of valid data points after the application of filtering criteria.

Period	Duration (hours)	Criteria (i) $Q_{Rn} < 0$	Criteria (ii) $t >$ Cutoff	Cutoff (hh:mm)	Criteria (iii) $\lvert TF \rvert \geq 1$
October	96	31	25	15:00	20
March	96	36	29	16:00	28

Figure 7 and the linear regression statistics (Table 2) show that all 3T-ET approaches tracked the dynamics of the corresponding reference ET_o values reasonably well ($R^2 > 0.659$), indicating a good response from the 3T method to changes in the local meteorological parameters and environmental setting. However, it is also clear that all 3T-ET approaches tended to overestimate ET relative to the corresponding reference ET_o values, with PBIAS ranging from 24.4 to 81.1% (Table 2).

Table 2. Quality metrics for 3T-ET predictions compared with the reference ET_o for the October and March preferred periods. Visualisations of the simple linear regressions are presented in Supplementary Material E.

Period	Metric	ET1	ET2	ET3	ET4
October	Mean Absolute Error, MAE ($mm \cdot h^{-1}$)	0.14	0.15	0.15	0.12
	Mean Absolute Percentage Error, MAPE (%)	83.3	84.7	84.4	69.0
	Percentage Bias, PBIAS (%)	79.0	81.1	80.4	62.4
	Linear Regression Slope, m (-)	1.84	1.87	1.86.	1.67
	Lin. Reg. Coefficient of Determination, R^2 (-)	0.668	0.659	0.663	0.663
March	MAE ($mm \cdot h^{-1}$)	0.07	0.06	0.07	0.05
	MAPE (%)	72.6	66.8	48.3	39.2
	PBIAS (%)	66.0	60.7	38.2	24.4
	m (-)	1.71	1.65	1.42	1.28
	R^2 (-)	0.874	0.856	0.854	0.854

It should be noted that these ET_o values are not 'actual' ET rates, but they serve as a useful benchmark for evaluating the magnitude of 3T-ET estimates. Future research should also quantify 'actual' ET, e.g., via direct measurements using a lysimeter in a similar approach to Zhang et al. [14], to provide more definitive comparisons to 3T-ET-derived estimates.

In the present study, ET1 and ET2 generally produced the highest estimates, and ET3 and ET4 consistently produced estimates closer to the corresponding ET_o values. This is particularly evident in the March data (Figure 7b, Table 2). ET3 estimates were closer to ET_o values compared to the ET2 estimates, even though both approaches assumed that $Q_{Rn,veg}$ and $Q_{Rn,imt}$ were the same. This demonstrates that the chosen values of α and ϵ used in ET1 and ET2 may require refinement if those approaches are to reliably estimate ET. Note that the 3T-ET1 estimates presented in Figure 7 used the default values of albedo (0.230) and emissivity (0.900) for short grass to estimate $Q_{Rn,imt}$. Representative values of albedo (0.110) and emissivity (0.950) for artificial grass have been provided by Loveday et al. [29] and Yaghoobian et al. [30], respectively. However, the use of these alternative values led to very minor changes in the overall performance of 3T-ET1, with the MAPE with respect to ET_o increasing from 83.3 to 88.3% in October and from 72.7 to 74.9% in March. For clarity, this dataset is not included in Figure 7.

The fact that ET4 values were noticeably above ET_o but consistently lower than any of the other three approaches, suggests that soil heat flux density loss should not be ignored at the hourly timestep for the 3-T method.

The elevated 3T-ET estimates, in comparison to the ET_o estimates from FAO-56 PM, may suggest that the 3T method used in this study has overestimated the $Q_{LE,veg}$ component in the surface energy balance for the vegetated surface. There are a number of possible reasons why the $Q_{LE,veg}$ component in the 3T equation for this study may be too high, each of which may warrant further exploration:

- The Q_{Soil}:Q_{Rn} ratio used to estimate the Q_{Rn} for the surfaces was too low. Santanello and Friedl [31] demonstrate that the Q_{Soil}:Q_{Rn} ratio can vary anywhere between 0.3 and −0.2 for sandy soil covered by vegetation between 07:00 and 16:00. Any Q_{Soil}:Q_{Rn} ratio should be justified through actual soil heat flux values measured in the subsurface;
- The measured T_{imt} values were significantly higher compared to the T_{veg} for the majority of timesteps during the day-time. Other than the evaporative cooling effect, the differences in specific heat capacity and material compositions between these two surfaces could contribute to this temperature difference, impacting both the temperature fraction and estimation of $Q_{Rn,imt}$;
- An air temperature gradient could have been present where T_{air} may change appreciably at different heights between the vegetation surface and at the observation height (0.260 or 0.600 m) used in this study. If T_{air} at the observed height was consistently warmer compared to the air temperature immediately above the vegetated surface, this would lead to higher $Q_{LE,veg}$ estimates.

Alternatively, it is possible that the 3T estimates are correct or at least closer to the actual ET than ET_o and that the reference ET_o is not a good representation of the actual test bed ET. While the vegetation type was selected to reflect short-cut grass and was maintained in a well-watered condition, the small size of the test bed is not representative of the large homogeneous area assumed in Allen et al. [24]. Instead, it is possible that real microclimate effects associated with the small footprint of the test bed and its exposed rooftop location caused actual ET to deviate from ET_o. Ouédraogo et al. [32] highlighted actual ET rates (as measured via a lysimeter) that consistently exceeded ET_o in a comparable experimental setting. Such local microclimate effects could mean that a location factor, K_l, analogous to a crop factor may be required to characterise the expected ET in this specific locational context. The development of the 3T method, as explored here, should contribute to the further understanding of how local environmental settings influence actual ET rates in complex, heterogeneous, urban environments.

4. Conclusions

This study has explored the application of the three-temperatures (3T) method for evapotranspiration (ET) estimation over a relatively small, homogenous, vegetated surface located in an urban environment using plastic artificial grass as the imitation surface.

Reasonable 3T-ET hourly estimates were achieved over the experimental period, to the extent that the hourly 3T-ET estimates responded well to changes in the local microclimate conditions and tracked trends in the corresponding hourly reference ET (ET_o) values. However, the 3T-ET estimates were very sensitive to changes in imitation surface temperature (T_{imt}) and air temperature (T_{air}), specifically when the values of these parameters converged, leading to an increasingly high temperature fraction. This is a key limitation of the 3T method, typically restricting valid 3T-ET estimates to between mid-morning and late afternoon when there is a clear difference between T_{imt} and T_{air}.

In light of these observations, filtering the data to daylight hours and excluding periods of building shadows and extreme temperature fraction values led to improved 3T-ET estimates, where the most of the estimates were within 1 order of magnitude compared with corresponding ET_o values. However, the majority of the 3T-ET hourly estimates were

greater than ET_o (mean absolute error, MAE, of 0.05 to 0.15 mm·h^{-1}). These deviations were marginally reduced in the ET3 method using monitored net-radiation values ($Q_{Rn,veg}$) (March MAE, 0.05 mm·h^{-1}) rather than estimating imitation surface net radiation ($Q_{Rn,imt}$) from T_{imt} using values of albedo (α) and emissivity (ϵ) from the literature, as per the ET1 and ET2 methods (March MAE, 0.07 and 0.06 mm·h^{-1}, respectively). Further reductions in error were achieved in ET4 through the incorporation of soil heat flux into the 3T method (March MAE, 0.03 mm·h^{-1}).

While the preliminary work presented here has demonstrated the potential for a portable ET measurement system that might be deployed to quantify ET rates from urban SuDS/GI, the uncertainties highlighted here suggest that more work is required before the 3T-ET method can be recommend as a robust approach for practical deployment.

Future research should be undertaken to repeat elements of this 3T-ET study and compare the estimates against measured 'actual' ET values determined by direct methods (e.g., by mass loss) over continuous monitoring periods. Away from the equator, these trials should be undertaken during the summer months when ET rates are expected to be at their highest, day lengths are longer, and solar inclination angles are larger, thereby reducing building shadow effects. The quantification of the soil heat flux density component of the surface energy balance should also be undertaken over a diurnal cycle to rationalise sub-daily 3T-ET estimates. Further investigation should be directed towards evaluating the effects of different imitation surfaces in the 3T method. Furthermore, a better understanding of the vertical air temperature profile above the vegetated surface is required in order to identify the optimal placement of air temperature instrumentation in the 3T method.

Supplementary Materials: The following supporting information can be downloaded at https://www.mdpi.com/article/10.3390/hydrology12120315/s1. Supplementary Material Section A: Instrument Accuracy and Precision Summary; Supplementary Material Section B: Estimated vs. Measured Shortwave, Longwave and Net Radiation; Supplementary Material Section C: Three-Temperatures, Temperature Fraction and Evapotranspiration (ET1) Data for the Complete Study Period; Supplementary Material Section D: Building Shadows and Reflections from Adjacent Surfaces; Supplementary Material Section E: Simple Linear Regressions between Reference ET and 3T-ET.

Author Contributions: Conceptualization, B.W., S.D.-V., and V.S.; methodology, B.W., S.D.-V., and V.S.; validation, B.W.; formal analysis, B.W.; investigation, B.W., S.D.-V., and V.S.; data curation, B.W.; writing—original draft preparation, B.W.; writing—review and editing, S.D.-V. and V.S.; visualization, B.W. and S.D.-V.; supervision, S.D.-V. and V.S.; project administration, V.S.; funding acquisition, B.W. and V.S. All authors have read and agreed to the published version of the manuscript.

Funding: This research was funded by the Engineering and Physical Sciences Research Council (EPSRC) DTP, grant number EP/W524360/1; project number: 2779460.

Data Availability Statement: The raw data collected as part of this study are openly available from the University of Sheffield's research data repository (ORDA) at https://doi.org/10.15131/shef.data.30327661.

Conflicts of Interest: The authors declare no conflicts of interest.

Abbreviations and Notation

The following abbreviations and notation are used in this manuscript:

3T	Three-Temperatures method
ET	Evapotranspiration
FAO	Food and Agriculture Organization
GI	Green Infrastructure
MAE	Mean Absolute Error

PBIAS	Percentage Bias	
PM	Penman–Monteith	
RMSE	Root Mean Squared Error	
SuDS	Sustainable Drainage Systems	
α	Albedo (Surface Reflectivity)	-
ϵ	Emissivity	-
λ	Latent Heat of Vaporisation	$J.kg^{-1}$
ρ_w	Density of Water	$kg.m^{-3}$
σ	Stefan–Boltzmann Constant (5.6697×10^{-8})	$W.m^{-2}.K^{-4}$
τ	Kendall Correlation Coefficient	-
dt	Timestep (3600 s for Hourly Calculations)	s
$ET_{3T,dt}$	Evapotranspiration Rate Estimated by the 3T Method	$mm.h^{-1}$
ET_o	Reference Evapotranspiration Derived from FAO-56 PM	$mm.h^{-1}$
m	Slope of a Simple Linear Regression	-
$Q_{LE,veg}$	Latent Heat Flux Density from Vegetated Surface	$W.m^{-2}$
Q_{Rn}	Net Radiation	$W.m^{-2}$
$Q_{Rn,imt}$	Net Radiation from Imitation Surface	$W.m^{-2}$
$Q_{Rn,lw}$	Net Longwave Radiation	$W.m^{-2}$
$Q_{Rn,sw}$	Net Shortwave Radiation	$W.m^{-2}$
$Q_{Rn,veg}$	Net Radiation from Vegetated Surface	$W.m^{-2}$
Q_{Soil}	Soil Heat Flux Density	$W.m^{-2}$
R^2	Coefficient of Determination of a Simple Linear Regression	-
RH	Relative Humidity	%
$\downarrow R_{lw}$	Incoming Longwave Radiation	$W.m^{-2}$
$\uparrow R_{lw}$	Outgoing Longwave Radiation	$W.m^{-2}$
$\downarrow R_{solar}$	Incoming Solar (Shortwave) Radiation	$W.m^{-2}$
t	Time of Day	hh:mm
T	Surface Temperature	K
T_{air}	Air Temperature	°C
T_{imt}	Imitation Surface Temperature	°C
T_{veg}	Vegetated Surface Temperature	°C
TF	Temperature Fraction	-
u	Wind Speed	$m.s^{-1}$

References

1. Novák, V. *Evapotranspiration in the Soil-Plant-Atmosphere System*; Springer: Dordrecht, The Netherlands, 2012. [CrossRef]
2. Muthanna, T.M.; Viklander, M.; Thorolfsson, S.T. Seasonal climatic effects on the hydrology of a rain garden. *Hydrol. Process.* **2008**, *22*, 1640–1649. [CrossRef]
3. Wadzuk, B.M.; Asce, M.; Schneider, D.; Feller, M.; Traver, R.G. Evapotranspiration from a Green-Roof Storm-Water Control Measure. *J. Irrig. Drain. Eng.* **2013**, *139*, 995–1003. [CrossRef]
4. Szota, C.; McCarthy, M.J.; Sanders, G.J.; Farrell, C.; Fletcher, T.D.; Arndt, S.K.; Livesley, S.J. Tree water-use strategies to improve stormwater retention performance of biofiltration systems. *Water Res.* **2018**, *144*, 285–295. [CrossRef] [PubMed]
5. Hess, A.; Wadzuk, B.; Welker, A. Evapotranspiration estimation in rain gardens using soil moisture sensors. *Vadose Zone J.* **2021**, *20*, e20100. [CrossRef]
6. De-Ville, S.; Edmondson, J.; Green, D.; Stirling, R.; Dawson, R.; Stovin, V. Effect of vegetation treatment and water stress on evapotranspiration in bioretention systems. *Water Res.* **2024**, *252*, 121182. [CrossRef]
7. Shuttleworth, W.J. Evapotranspiration measurement methods. *Southwest Hydrol.* **2008**, *7*, 22–23.
8. Abtew, W.; Melesse, A. *Evaporation and Evapotranspiration: Measurements and Estimations*; Springer: Dordrecht, The Netherlands, 2013. [CrossRef]
9. Baldocchi, D.D. Assessing the eddy covariance technique for evaluating carbon dioxide exchange rates of ecosystems: Past, present and future. *Glob. Change Biol.* **2003**, *9*, 479–492. [CrossRef]

10. De Bruin, H.; Wang, J. Scintillometry: A Review. *Researchgate* **2017**. Available online: https://www.researchgate.net/publication/316285424_Scintillometry_a_review (accessed on 14 October 2025).
11. Berger, D.L.; Johnson, M.J.; Tumbusch, M.L.; Mackay, J. *Estimates of Evapotranspiration from the Ruby Lake National Wildlife Refuge Area, Ruby Valley, Northeastern Nevada, May 1999–October 2000*; Technical Report; U.S. Geological Survey: Carson, NV, USA, 2001. [CrossRef]
12. Heilman, J.; Brittin, C.; Neale, C. Fetch requirements for bowen ratio measurements of latent and sensible heat fluxes. *Agric. For. Meteorol.* **1989**, *44*, 261–273. [CrossRef]
13. Qiu, G.Y.; Yano, T.; Momii, K. Estimation of Plant Transpiration by Imitation Leaf Temperature. *Trans. Jpn. Soc. Irrig. Drain. Reclam. Eng.* **1996**, *1996*, 767–773. [CrossRef]
14. Zhang, Y.; Qin, H.; Zhang, J.; Hu, Y. An in-situ measurement method of evapotranspiration from typical LID facilities based on the three-temperature model. *J. Hydrol.* **2020**, *588*, 125105. [CrossRef]
15. Qiu, G.; Tan, S.; Wang, Y.; Yu, X.; Yan, C. Characteristics of evapotranspiration of urban lawns in a sub-tropical megacity and its measurement by the 'three temperature model + infrared remote sensing' method. *Remote Sens.* **2017**, *9*, 502. [CrossRef]
16. Qiu, G.Y.; Wang, B.; Li, T.; Zhang, X.; Zou, Z.; Yan, C. Estimation of the transpiration of urban shrubs using the modified three-dimensional three-temperature model and infrared remote sensing. *J. Hydrol.* **2021**, *594*, 125940. [CrossRef]
17. Tian, F.; Qiu, G.; Lü, Y.; Yang, Y.; Xiong, Y. Use of high-resolution thermal infrared remote sensing and "three-temperature model" for transpiration monitoring in arid inland river catchment. *J. Hydrol.* **2014**, *515*, 307–315. [CrossRef]
18. Yan, C.; Ding, J.; Wang, B.; Qin, L.; Shi, Z.; Qiu, G.Y. An in-situ measurement and assessment of evaporative cooling effects of low impact development facilities in a subtropical city. *Agric. For. Meteorol.* **2023**, *332*, 109363. [CrossRef]
19. Zou, Z.; Yang, Y.; Qiu, G.Y. Quantifying the Evapotranspiration Rate and Its Cooling Effects of Urban Hedges Based on Three-Temperature Model and Infrared Remote Sensing. *Remote Sens.* **2019**, *11*, 202. [CrossRef]
20. Leinonen, I.; Grant, O.M.; Tagliavia, C.P.P.; Chaves, M.M.; Jones, H.G. Estimating stomatal conductance with thermal imagery. *Plant Cell Environ.* **2006**, *29*, 1508–1518. [CrossRef]
21. Apolo-Apolo, O.E.; Martínez-Guanter, J.; Pérez-Ruiz, M.; Egea, G. Design and assessment of new artificial reference surfaces for real time monitoring of crop water stress index in maize. *Agric. Water Manag.* **2020**, *240*, 106304. [CrossRef]
22. Jones, H.G.; Hutchinson, P.A.; May, T.; Jamali, H.; Deery, D.M. A practical method using a network of fixed infrared sensors for estimating crop canopy conductance and evaporation rate. *Biosyst. Eng.* **2018**, *165*, 59–69. [CrossRef]
23. Caine, R.S.; Khan, M.S.; Brench, R.A.; Walker, H.J.; Croft, H.L. Inside-out: Synergising leaf biochemical traits with stomatal-regulated water fluxes to enhance transpiration modelling during abiotic stress. *Plant Cell Environ.* **2024**, *47*, 3494–3513. [CrossRef]
24. Allen, R.G.; Pereira, L.S.; Raes, D.; Smith, M. *Crop Evapotranspiration: Guidelines for Computing Crop Water Requirements*; FAO Irrigation and Drainage Paper 56; Food and Agriculture Organization of the United Nations: Rome, Italy, 1998.
25. Department for Environment Food & Rural Affairs (DEFRA). Real Time Flood Monitoring Data: Archives. 2025. Available online: https://environment.data.gov.uk/flood-monitoring/archive (accessed on 14 October 2025).
26. Oke, T.R.; Mills, G.; Christen, A.; Voogt, J.A. *Urban Climates*, 1st ed.; Cambridge University Press: Cambridge, UK, 2017. [CrossRef]
27. Grant, I.F.; Prata, A.J.; Cechet, R.P. The Impact of the Diurnal Variation of Albedo on the Remote Sensing of the Daily Mean Albedo of Grassland. *J. Appl. Meteorol.* **2000**, *39*, 231–244. [CrossRef]
28. Chen, C. Determining the Leaf Emissivity of Three Crops by Infrared Thermometry. *Sensors* **2015**, *15*, 11387–11401. [CrossRef] [PubMed]
29. Loveday, J.; Loveday, G.K.; Byrne, J.J.; Ong, B.l.; Morrison, G.M. Modified iButtons: A Low-Cost Instrument to Measure the Albedo of Landscape Elements. *Sustainability* **2019**, *11*, 6896. [CrossRef]
30. Yaghoobian, N.; Kleissl, J.; Krayenhoff, E.S. Modeling the Thermal Effects of Artificial Turf on the Urban Environment. *J. Appl. Meteorol. Climatol.* **2010**, *49*, 332–345. [CrossRef]
31. Santanello, J.A.; Friedl, M.A. Diurnal Covariation in Soil Heat Flux and Net Radiation. *J. Appl. Meteorol.* **2003**, *42*, 851–862. [CrossRef]
32. Ouédraogo, A.A.; Berthier, E.; Durand, B.; Gromaire, M.C. Determinants of Evapotranspiration in Urban Rain Gardens: A Case Study with Lysimeters under Temperate Climate. *Hydrology* **2022**, *9*, 42. [CrossRef]

Disclaimer/Publisher's Note: The statements, opinions and data contained in all publications are solely those of the individual author(s) and contributor(s) and not of MDPI and/or the editor(s). MDPI and/or the editor(s) disclaim responsibility for any injury to people or property resulting from any ideas, methods, instructions or products referred to in the content.